

**Evaluation of 18F-FDG PET and DWI datasets  
for the prediction of therapy response of soft tissues sarcomas  
under neoadjuvant isolated limb perfusion.**

Michal Chodyla, MD<sup>1</sup>; Aydin Demircioglu, PhD<sup>1</sup>; Benedikt M. Schaarschmidt, MD<sup>1</sup>; Stefanie Bertram, MD<sup>2</sup>; Nils Martin Bruckmann, MD<sup>3</sup>; Jennifer Haferkamp<sup>1</sup>; Yan Li, MD<sup>1</sup>; Sebastian Bauer, MD<sup>4</sup>; Lars Podleska, MD<sup>5</sup>; Christoph Rischpler, MD<sup>6</sup>; Michael Forsting, MD<sup>1</sup>; Ken Herrmann, MD<sup>6</sup>; Lale Umutlu, MD<sup>1</sup>; Johannes Grueneisen, MD<sup>1,\*</sup>

**Affiliations**

<sup>1</sup>Department of Diagnostic and Interventional Radiology, University Hospital Essen, University of Duisburg-Essen, Germany

<sup>2</sup>Institute of Pathology, University Hospital Essen, University of Duisburg-Essen, Germany

<sup>3</sup>Department of Diagnostic and Interventional Radiology, University Hospital Dusseldorf, University of Dusseldorf, Germany

<sup>4</sup>Sarcoma Center, Western German Cancer Center, University of Duisburg-Essen, Germany

<sup>5</sup>Sarcoma Surgery Division, Department of General, Visceral and Transplantation Surgery, University Hospital Essen, University of Duisburg-Essen, Germany

<sup>6</sup>Department of Nuclear Medicine, University Hospital Essen, University of Duisburg-Essen, Germany

\*Corresponding author:

Johannes Grueneisen, MD

University Hospital Essen

Department of Diagnostic and Interventional Radiology

Hufelandstrasse 55, 45147 Essen, Germany

Email: Johannes.grueneisen@uk-essen.de

Phone: +49(0)201/723-1501

**Total word count**

4963 words

**Short running title**

PET/MRI for response prediction of ILP

## **Abstract**

### **Purpose**

To evaluate and compare the clinical utility of simultaneously obtained quantitative 18F-fluorodeoxyglucose positron-emission-tomography (18F-FDG PET) and diffusion-weighted imaging (DWI) datasets for the prediction of histopathological therapy response of soft tissue sarcomas (STS) under neoadjuvant isolated limb perfusion (ILP).

### **Methods**

A total of 37 patients with confirmation of a STS of the extremities underwent an 18F-FDG PET/magnetic resonance imaging (MRI) examination before (1<sup>st</sup> scan) and after (2<sup>nd</sup> scan) ILP with melphalan and TNF- $\alpha$ . For each patient, the maximum tumor size, metabolic activity (standardized uptake values, SUV) and diffusion-restriction (apparent diffusion restriction values, ADC) were determined in pre- and posttherapeutic examinations and percentage changes during treatment were calculated. A Mann-Whitney U test was used and receiver operating characteristic (ROC) analysis was performed to compare the results of the different quantitative parameters to predict histopathological therapy response. Results from histopathological analysis after subsequent tumor resection served as reference standard and patients were defined as responders/non-responders based on the grading scale by Salzer-Kuntschik.

### **Results**

Histopathological analysis categorized 22 (59%) patients as therapy responders (Grade I-III) and 15 (41%) patients as non-responders (Grade IV-VI). Tumors in the responder group

showed a mean reduction in size of -9.7% and metabolic activity (SUVpeak: -51.9%; SUVmean: -43.8%) as well as an increase of the ADC values (ADCmin: +29.4% and ADCmean: +32.8%) under treatment. Percentage changes in the non-responder group amounted to: tumor size -6.2%; SUVpeak: -17.3%; SUVmean: -13.9%; ADCmin: +15.3% and ADCmean: +14.6%. Changes of the SUVs and ADCmean values between responders and non-responders were significantly different ( $<0.01$ ), whereas differences in tumor size and the ADCmin values did not reach significance level ( $>0.05$ ). The corresponding AUCs were 0.63 (tumor size), 0.87 (SUVpeak), 0.82 (SUVmean), 0.63 (ADCmin), 0.84 (ADCmean) and 0.89 (ratio: ADCmean/SUVpeak), respectively.

## **Conclusion**

$^{18}\text{F}$ -FDG PET and MR-derived quantitative imaging parameters (SUVs and ADCmean) and their combination reveal a good performance for the prediction of histopathological therapy response of STS under neoadjuvant ILP. Therefore, integrated PET/MRI could serve as a valuable tool for pretherapeutic assessment as well as monitoring of neoadjuvant treatment strategies of STS.

## **Key words**

Soft-tissue sarcoma, isolated limb perfusion,  $^{18}\text{F}$ -FDG PET, DWI, therapy response prediction

## Introduction

Limb salvage is a major goal for patients with diagnosed soft-tissue sarcomas (STS) of the extremities. Therefore, neoadjuvant treatment strategies are frequently applied for primary non-resectable tumor manifestations, in order to achieve local tumor control and complete tumor resection (1). In this context, it has been demonstrated that good clinical outcome, in terms of high limb salvage rates and a reduced number of locoregional tumor recurrences, necessitates good histopathological tumor response under neoadjuvant therapy and equals limb amputation considering patients' survival (2,3).

Hyperthermic isolated limb perfusion (ILP) with tumor necrosis factor- $\alpha$  (TNF- $\alpha$ ) and melphalan has been shown to be an efficient preoperative treatment procedure for STS to ensure local disease regression (4,5). This technique enables the administration of high regional drug concentrations with limb salvage rates above 70% (6). However, there is generally a need to reliably assess treatment success prior to subsequent tumor resection, in order to consider further therapeutic interventions, if the initial treatment effects were not sufficient.

In clinical routine, size- and morphology-based therapy monitoring is commonly applied, yet, has not been shown appropriate for reliable response evaluation of STS (7). Some previous studies already investigated the use of  $^{18}\text{F}$ -fluorodeoxyglucose ( $^{18}\text{F}$ -FDG) positron-emission-tomography (PET) data for response assessment of STS and reported better results than for size and volumetric tumor measurements (8-10). Besides morphologic and metabolic imaging datasets, integrated PET/magnetic resonance imaging (MRI) scanners allow for the simultaneous acquisition of further functional imaging parameters. Diffusion-weighted imaging (DWI) has been widely established in oncological imaging and provides information about the composition and structure of biological tissues (11,12).

Therefore, it has previously been shown that the DWI-derived apparent diffusion coefficient (ADC) can be applied as a quantitative imaging biomarker for predicting and monitoring therapeutic effects of solid tumors (13,14). Accordingly, this study targeted to evaluate and directly compare the potential of PET/MR-based quantitative imaging parameters as well as their combination for response assessment of STS under neoadjuvant ILP.

## **Material and Methods**

### **Patients**

The institutional review board approved this study and all patients signed a written informed consent before each examination. A total of 37 patients (mean age  $51.8 \pm 12.5$  years) with primary ( $n=31$ ) or recurrent ( $n=6$ ) STS were included in this prospective study. All patients were enrolled for a  $^{18}\text{F}$ -FDG PET/MR examination within one week before the treatment procedure as well as for a second scan after neoadjuvant ILP (mean delay:  $44.3 \pm 8.6$  days) and prior to subsequent tumor resection. Table 1 gives an overview about the different STS subtypes included in this study.

### **Isolated limb perfusion**

Neoadjuvant ILP was performed under general anesthesia and mild hyperthermia of  $39^\circ$ . For tumors of the upper limb a vascular access via a brachial or axillar approach was chosen and for STS manifestations of the lower limb a femoral or iliac approach was used. As a first step, recombinant human TNF- $\alpha$  (Beromun, Boehringer-Ingelheim, Germany) was applied, adjusted to 0.25 mg/L perfused tissue volume and with a delay of 15 minutes

melphalan (L-phenylalanine mustard) was administered at a concentration of 11mg per liters of limb volume for legs and 13mg/L per liters of limb volume for arms. Continuous leakage monitoring was performed with the assistance of nuclear medicine testing with radio-labeled serum (Indium-111).

## **PET/MRI**

All PET/MR examinations were acquired on a 3 Tesla Biograph mMR scanner (Siemens Healthineers, Germany) in supine position and with a delay of 60 minutes after a body weight-adapted dosage of 18F-FDG was administered intravenously (mean activity: 245±33 MBq (1<sup>st</sup> scan) and 237±35 MBq (2<sup>nd</sup> scan)). PET/MRI datasets were obtained in 1-2 bed positions covering the entire tumor volume with 10 minutes PET-data acquisition time per bed-position.

Image reconstruction was performed subsequently using the iterative ordered-subset expectation maximization algorithm, 3 iterations and 21 subsets, a Gaussian filter with 4 mm full width at half maximum and a 344 x 344 image matrix. PET images were automatically attenuation corrected based on a four-compartment-model attenuation map ( $\mu$ -map) calculated from fat-only and water-only datasets, as obtained by Dixon-based sequences, facilitating a segmentation into background, lung, fat, and soft tissue. MR data acquisition was performed simultaneously to PET imaging using dedicated mMR body phased array coils and mMR spine coils and the following sequence protocol: a coronal 3-dimensional volume interpolated breath-hold examination (VIBE) sequence, a coronal short tau inversion recovery sequence, a transversal T1 weighted (w) turbo-spin echo (TSE) sequence, a transversal T2w TSE sequence, a transversal diffusion-weighted echo-planar imaging sequence and a fat-saturated transversal 3-dimensional VIBE sequence for dynamic

imaging. Therefore, intravenous contrast agent (0.1 mmol/kg bodyweight Gadobutrol, Bayer Healthcare, Germany) was administered and three repetitive scans were acquired at a delay of 25, 54 and 86 seconds. Additionally, transversal and coronal post-contrast fat-saturated T1w TSE sequences were acquired. Detailed information about the MRI sequence parameters are given in the Supplemental Table 1.

### **Data analysis**

Two experienced physicians with 7 and 8 years of experience in reading MRI and hybrid imaging, analyzed the acquired PET/MR imaging datasets in consensus, using a dedicated viewing software for hybrid imaging (Syngo.via B30; Siemens Healthineers, Germany). Both readers were informed about patients' diagnosis and the treatment procedure, but they were blinded regarding the results of histopathological analysis after subsequent tumor resection.

In a first step, the readers were instructed to determine the maximum tumor diameter on contrast-enhanced fat-saturated T1w MR images in pre- and posttherapeutic PET/MR examinations for each patient. For the evaluation of diffusion-restriction of the STS manifestations, an ADC map was generated by the scanner software (Syngo MR B18P, Siemens Healthineers, Germany) using three different b-values ( $b = 0 \text{ s/mm}^2$ ,  $b = 500 \text{ s/mm}^2$ ,  $b = 1000 \text{ s/mm}^2$ ). The tumor lesions were identified on diffusion-weighted sequences and a polygonal region of interest (ROI) was manually drawn on every slice on the corresponding ADCmap, covering the entire tumor lesion. After visual confirmation of a correct placement, ADC values were determined. Furthermore, measurements of the metabolic activity of the STS manifestations were performed. Therefore, a polygonal ROI was manually drawn on every slice on fused PET/MR images, covering the entire tumor volume and the SUVpeak

(average SUV within a spherical VOI of 1 cm<sup>3</sup> around the hottest point in the tumor) as well as the SUV<sub>mean</sub> were obtained.

### **Reference standard**

For the determination of treatment response/non-response of STS to neoadjuvant ILP, histopathological analysis of surgical specimen after subsequent tumor resection served as the reference standard. Therefore, microscopic analysis was performed on hematoxylin and eosin-stained slides and in each case tumor regression was assessed by light microscopy according to the grading scale by Salzer-Kuntschik (15). Based on the percentage of viable tumor amount, histopathological findings were subdivided into six different stages (grade I = no vital tumor, grade II = single vital tumor cell or one cluster/5 mm, grade III < 10% vital tumor, grade IV = 10–50% vital tumor, grade V > 50% vital tumor and grade VI = no effect of therapy). In accordance with previous publications, tumor stages I-III were categorized as histopathological responders and stages IV-VI as non-responders (7,16).

### **Statistical analysis**

Statistical analysis was performed using the R software environment for statistical computing and graphics (version 3.6.1). Quantitative PET- and MR-derived parameters and their percentage changes under therapy are presented as mean values ± standard deviation (SD). In addition, for each tumor the ratio of the ADC<sub>mean</sub> and the SUV<sub>peak</sub> (ADC<sub>mean</sub>/SUV<sub>peak</sub>) in pre- and posttherapeutic PET/MR examinations as well as their percentage changes under treatment were calculated. A Mann-Whitney U test was applied

to test for significant differences of the results between the histopathological responder and non-responder group. P-values  $<0.05$  were considered to be statistically significant. Furthermore, receiver operating characteristic (ROC) analysis was performed and the area under the curve (AUC) values as well as the optimal thresholds were calculated for the quantitative parameters to predict treatment response under ILP. For statistical comparison of different AUC curves, a bootstrap test with 2000 replicates was used.

## **Results**

### **Patients**

All patients successfully completed the pre- and posttherapeutic PET/MR examinations without any relevant side effects. Histopathological analysis after subsequent tumor resection categorized 22 (59%) patients as therapy responders (regression grade I-III) and 15 (41%) patients as non-responders (regression grade IV-VI). Tumor grades as well as histological findings of all 37 patients are shown in Table 2 and in the Supplemental Table 2.

### **Quantitative image analysis**

Table 3 shows the calculated mean values and percentage changes of the different  $^{18}\text{F}$ -FDG PET- and MR-derived quantitative imaging parameters for histopathological therapy responders and non-responders. The responder group revealed a significant and stronger decrease of the standardized uptake values (p-values: SUV<sub>mean</sub>, 0.001; SUV<sub>peak</sub>,

< 0.001) and for the ratio ADCmean/SUVpeak (p-value: < 0.001) as well as a stronger increase of the ADCmean values (p-value < 0.001), when compared to the results obtained from the non-responder group (Figs. 1 and 2). On the other hand, differences of the calculated mean values for tumor size (p-value: 0.191) and the ADCmin (p-value: 0.202) did not reach significant level between histopathological therapy responders and non-responders.

According to ROC-analysis for the prediction of histopathological treatment response to neoadjuvant ILP, the AUC value of the SUVpeak was slightly and not-significantly higher than the AUC values of the ADCmean and SUVmean, but differed significantly from the results for tumor size and the ADCmin (Table 4, Fig. 3). In addition, a significantly higher AUC value was obtained for the ADCmean, when compared with the results for the ADCmin. Moreover, the ratio of the 18F-FDG PET -and DWI-derived imaging parameters with the best predictive values (SUVpeak and ADCmean) was calculated. The results for ADCmean/SUVpeak revealed the highest AUC value among the different variables, but differences to the results of the SUVpeak, ADCmean and SUVmean were not significant.

Calculated optimal thresholds for percentage changes of the quantitative variables to discriminate between a histopathological therapy response and non-response amounted to: -4.11% for tumor size, -34.44% for the SUVmean, -43.82% for the SUVpeak, 25.39% for the ADCmin, 20.41% for the ADCmean and 98.09% for the ratio ADCmean/SUVpeak, respectively.

## Discussion

Hyperthermic ILP with TNF-alpha and melphalan has been proven to be a highly effective neoadjuvant treatment procedure for locally advanced STS of the extremities, in order to achieve local tumor control and limb preserving surgery (4,5). Good histopathological tumor response, defined as less than 10% of viable tumor cells after therapy, is known to be associated with a reduced number of local tumor recurrences as well as higher limb salvage rates (2,7,16). In the present study, histopathological analysis revealed more than 90% tumor regression in 22/37 (59%) patients after ILP. A potential explanation for this moderate response rate is the inclusion of a heterogeneous study population, comprising patients with primary and recurrent sarcoma manifestations. Furthermore, it has been shown, that different subtypes of STS have variable response rates to ILP (3). In a study by Grabellus et. al, synovial sarcomas, spindle cell sarcomas, liposarcomas, epitheloid sarcoma and malignant peripheral nerve sheath tumors, which account for more than 50% of the included entities in the present study, revealed only a moderate extent of tumor regression (3). Therefore, presurgical evaluation of initial treatment success is of importance, to consider further therapeutic interventions, when neoadjuvant treatment effects were not sufficient.

MRI is the recommended and most commonly applied imaging modality for pre-surgical planning as well as treatment monitoring of STS of the extremities (17,18). However, previous studies demonstrated that morphological criteria, e.g. according to RECIST, do not allow for a reliable response assessment of STS to neoadjuvant therapeutic interventions (7,19). In accordance with these findings, our results reveal only a weak correlation between a solely size-based response evaluation and therapy induced histopathological changes.

STS commonly show structural changes, in terms of the development of fibrosis, granulation tissue and necrosis as an initial histological therapeutic effect, which frequently precedes noticeable changes in tumor size (20).

Moreover, the introduction of DWI as an additional functional parameter to morphologic MR imaging has been demonstrated to facilitate significant improvements in tumor detection and noninvasive characterization of biologic tissues (21-23). Based on the restricted motion of water molecules within cancer lesions, caused by higher cell densities, DWI-derived ADC values have been recognized as valuable quantitative parameters for the assessment of tissue compositions and can be applied as an imaging biomarker for predicting and monitoring therapeutic effects of solid tumors (24,25). In the present study, significant differences of percentage changes for the ADC<sub>mean</sub> between the responder and non-responder group were found as well as a good performance of this parameter with a high AUC value (0.84) for histopathological therapy response prediction to ILP. The ADC<sub>mean</sub> enables the quantification of potential changes of the mean tumor cellularity under treatment, covering the entire volume of the STS manifestation. Hence, a therapy induced loss of viable tumor cells, accompanied with the induction of tumor necrosis, leads to a measurable increase of the ADC<sub>mean</sub> value, based on the higher fluid amount and the decrease of solid tumor parts. Accordingly, the ADC<sub>mean</sub> value provides valuable information about alterations in the tissue structure without invasive tissue sampling, which are also reflected by the regression grading scale of Salzer-Kuntschik (15). Hayashida et al. reported comparable results, showing a significantly stronger increase of the ADC<sub>mean</sub> values for histopathological responders when compared to non-responders, whereas no differences were found for volumetric measurements of the sarcomas between the two

groups under treatment (26). Baunin et al. could demonstrate that the ADC values increased significantly stronger in sarcoma patients with good pathological response even at a mid-course DW-MRI scan under chemotherapy, when compared to patients with poor response (27). In addition, Soldatos and colleagues could show, that adding functional MR sequences (e.g. DWI datasets) to a conventional MR imaging protocol, increases the sensitivity for the definition of treatment response of soft-tissue sarcomas (28). Surprisingly, our results revealed only a weak-association between the ADC<sub>min</sub> value and therapy induced histopathological changes. An explanation may be the structural heterogeneity of these frequently large tumor manifestations, whereby even small remaining solid tumor parts with restricted diffusivity have a relevant influence on this parameter. In addition, specific compositions of the different histological sarcoma subtypes as well as the occurrence of blood products due to hemorrhage after therapy might have affected ADC value measurements.

Furthermore, numerous publications have already demonstrated the high diagnostic performance of using 18F-FDG PET data for tumor staging as well as monitoring therapeutic effects of various cancers (29-31). Focusing on the evaluation of sarcoma patients, some studies could show, that the metabolic information based on 18F-FDG PET can be applied for the prediction of disease progression and survival of patients undergoing neoadjuvant systemic therapy (32-34). In addition, a few previous articles reported a more accurate therapy response assessment by 18F-FDG PET data quantifications than tumor size measurements (8-10,35). In our study, the SUV<sub>peak</sub> provided the best results among the different MR- and PET-derived quantitative imaging parameters for the prediction of treatment response, with a significantly higher AUC (0.87), when compared with the ADC<sub>min</sub>

(0.63) and tumor size (0.63). On the other hand, AUC values for the SUV<sub>peak</sub>, SUV<sub>mean</sub> and ADC<sub>mean</sub> differed only slightly and not significantly from each other. Buyn et al. reported a significant inverse correlation of percentage changes of the SUV and ADC values in osteosarcomas under neoadjuvant chemotherapy (36). In their work, the combination of SUV and ADC values was shown superior for prediction of good histologic response (0.85), when compared to SUV (0.77) and ADC values (0.73) alone (36). In concordance with these findings, the ratio ADC<sub>mean</sub>/SUV<sub>peak</sub> used in the present study revealed a tendency for more reliable treatment response evaluation, however, the results did not show significant differences, when compared with the two quantitative parameters alone. Accordingly, considering the complementary information of both imaging parameters, a combined analysis may enable a more sustainable histologic response assessment of STS under neoadjuvant treatment procedures.

Nevertheless, the present study is not without limitations. Based on the limited number of patients, the results have to be considered preliminary and need to be verified in larger patient cohorts. Furthermore, data analysis was performed in a consensus reading, hence, no specific data on interrater reliability could be collected. In addition, patients with primary tumors and recurrent sarcoma manifestations as well as different histopathological subtypes were included, which might have had an effect on the study results. Finally, as a standard procedure, histopathological analysis was performed on certain representative slices of the tumor manifestations, whereas, volumetric measurements of the quantitative imaging parameters were performed, which did not allow for a precise correlation between tissue histology and MR imaging data.

**Conclusion:**

Our study results demonstrate a good performance of <sup>18</sup>F-FDG PET and MR-derived quantitative imaging parameters (SUVs and ADC<sub>mean</sub>) for the prediction of histopathological therapy response of STS under neoadjuvant ILP. Especially, the combined and complementary information derived from these imaging features, reflecting different aspects of the underlying tumor biology, may provide more reliable evaluation of treatment effects of STS manifestations, when compared to sole morphological assessment. Therefore, integrated PET/MRI could serve as a valuable diagnostic tool for pretherapeutic and presurgical assessment as well as monitoring of neoadjuvant therapeutic strategies of STS.

**Disclosure**

Nothing to disclose.

**Conflict of Interest**

No potential conflicts of interest relevant to this article exist.

## KEY POINTS

### QUESTION:

Enable 18F-FDG PET- and MR-derived quantitative imaging parameters a reliable prediction of therapy response of STS under neoadjuvant ILP?

### PERTINENT FINDINGS:

In the present study, calculated mean values of the SUV<sub>peak</sub>, SUV<sub>mean</sub>, as well as the ratio ADC<sub>mean</sub>/SUV<sub>peak</sub> revealed a significantly stronger decrease and the ADC<sub>mean</sub> a stronger increase in the responder group, when compared to patients with histopathological non-response, whereas no significant differences were found for tumor size and the ADC<sub>min</sub> between both groups. In addition, ROC-analysis showed good results with high AUC values for the SUV<sub>peak</sub>, the ADC<sub>mean</sub> and the ratio ADC<sub>mean</sub>/SUV<sub>peak</sub> to predict histopathological treatment response, which differed significantly from the AUCs for tumor size or the ADC<sub>min</sub>.

### IMPLICATIONS FOR PATIENT CARE:

18F-FDG PET/MRI data may be valuable when implemented into diagnostic algorithms for the evaluation and prediction of treatment response of STS to neoadjuvant therapeutic interventions.

## References

1. Hohenberger P, Wysocki WM. Neoadjuvant treatment of locally advanced soft tissue sarcoma of the limbs: which treatment to choose? *Oncologist*. 2008;13:175-186.
2. Williard WC, Hajdu SI, Casper ES, Brennan MF. Comparison of amputation with limb-sparing operations for adult soft tissue sarcoma of the extremity. *Ann Surg*. 1992;215:269-275.
3. Grabellus F, Kraft C, Sheu-Grabellus SY, et al. Tumor vascularization and histopathologic regression of soft tissue sarcomas treated with isolated limb perfusion with TNF-alpha and melphalan. *J Surg Oncol*. 2011;103:371-379.
4. Eggermont AM, Schraffordt Koops H, Klausner JM, et al. Isolated limb perfusion with tumor necrosis factor and melphalan for limb salvage in 186 patients with locally advanced soft tissue extremity sarcomas. The cumulative multicenter European experience. *Ann Surg*. 1996;224:756-764.
5. Neuwirth MG, Song Y, Sinnamon AJ, Fraker DL, Zager JS, Karakousis GC. Isolated limb perfusion and infusion for extremity soft tissue sarcoma: a contemporary systematic review and meta-analysis. *Ann Surg Oncol*. 2017;24:3803-3810.
6. Verhoef C, de Wilt JH, Grunhagen DJ, van Geel AN, ten Hagen TL, Eggermont AM. Isolated limb perfusion with melphalan and TNF-alpha in the treatment of extremity sarcoma. *Curr Treat Options Oncol*. 2007;8:417-427.
7. Grabellus F, Stylianou E, Umutlu L, et al. Size-based clinical response evaluation is insufficient to assess clinical response of sarcomas treated with isolated limb perfusion with TNF-alpha and melphalan. *Ann Surg Oncol*. 2012;19:3375-3385.

8. Evilevitch V, Weber WA, Tap WD, et al. Reduction of glucose metabolic activity is more accurate than change in size at predicting histopathologic response to neoadjuvant therapy in high-grade soft-tissue sarcomas. *Clin Cancer Res.* 2008;14:715-720.
9. Denecke T, Hundsdorfer P, Misch D, et al. Assessment of histological response of paediatric bone sarcomas using FDG PET in comparison to morphological volume measurement and standardized MRI parameters. *Eur J Nucl Med Mol Imaging.* 2010;37:1842-1853.
10. Grueneisen J, Schaarschmidt B, Demircioglu A, et al. (18)F-FDG PET/MRI for therapy response assessment of isolated limb perfusion in patients with soft-tissue sarcomas. *J Nucl Med.* 2019;60:1537-1542.
11. Koh DM, Collins DJ. Diffusion-weighted MRI in the body: applications and challenges in oncology. *AJR Am J Roentgenol.* 2007;188:1622-1635.
12. Bonekamp S, Corona-Villalobos CP, Kamel IR. Oncologic applications of diffusion-weighted MRI in the body. *J Magn Reson Imaging.* 2012;35:257-279.
13. Padhani AR, Koh DM. Diffusion MR imaging for monitoring of treatment response. *Magn Reson Imaging Clin N Am.* 2011;19:181-209.
14. Schreuder SM, Lensing R, Stoker J, Bipat S. Monitoring treatment response in patients undergoing chemoradiotherapy for locally advanced uterine cervical cancer by additional diffusion-weighted imaging: a systematic review. *J Magn Reson Imaging.* 2015;42:572-594.
15. Salzer-Kuntschik M, Dellling G, Beron G, Sigmund R. Morphological grades of regression in osteosarcoma after polychemotherapy - study COSS 80. *J Cancer Res Clin Oncol.* 1983;106 Suppl:21-24.

16. Stacchiotti S, Collini P, Messina A, et al. High-grade soft-tissue sarcomas: tumor response assessment--pilot study to assess the correlation between radiologic and pathologic response by using RECIST and Choi criteria. *Radiology*. 2009;251:447-456.
17. De Schepper AM, De Beuckeleer L, Vandevenne J, Somville J. Magnetic resonance imaging of soft tissue tumors. *Eur Radiol*. 2000;10:213-223.
18. Noebauer-Huhmann IM, Weber MA, Lalam RK, et al. Soft tissue tumors in adults: ESSR-approved guidelines for diagnostic imaging. *Semin Musculoskelet Radiol*. 2015;19:475-482.
19. Canter RJ, Martinez SR, Tamurian RM, et al. Radiographic and histologic response to neoadjuvant radiotherapy in patients with soft tissue sarcoma. *Ann Surg Oncol*. 2010;17:2578-2584.
20. DeLaney TF, Spiro IJ, Suit HD, et al. Neoadjuvant chemotherapy and radiotherapy for large extremity soft-tissue sarcomas. *Int J Radiat Oncol Biol Phys*. 2003;56:1117-1127.
21. Low RN, Sebrechts CP, Barone RM, Muller W. Diffusion-weighted MRI of peritoneal tumors: comparison with conventional MRI and surgical and histopathologic findings--a feasibility study. *AJR Am J Roentgenol*. 2009;193:461-470.
22. Hong JH, Jee WH, Jung CK, Jung JY, Shin SH, Chung YG. Soft tissue sarcoma: adding diffusion-weighted imaging improves MR imaging evaluation of tumor margin infiltration. *Eur Radiol*. 2019;29:2589-2597.
23. Pickles MD, Gibbs P, Sreenivas M, Turnbull LW. Diffusion-weighted imaging of normal and malignant prostate tissue at 3.0T. *J Magn Reson Imaging*. 2006;23:130-134.
24. Liu Y, Bai R, Sun H, Liu H, Zhao X, Li Y. Diffusion-weighted imaging in predicting and monitoring the response of uterine cervical cancer to combined chemoradiation. *Clin Radiol*. 2009;64:1067-1074.

25. Wang L, Liu L, Han C, et al. The diffusion-weighted magnetic resonance imaging (DWI) predicts the early response of esophageal squamous cell carcinoma to concurrent chemoradiotherapy. *Radiother Oncol*. 2016;121:246-251.
26. Hayashida Y, Yakushiji T, Awai K, et al. Monitoring therapeutic responses of primary bone tumors by diffusion-weighted image: initial results. *Eur Radiol*. 2006;16:2637-2643.
27. Baunin C, Schmidt G, Baumstarck K, et al. Value of diffusion-weighted images in differentiating mid-course responders to chemotherapy for osteosarcoma compared to the histological response: preliminary results. *Skeletal Radiol*. 2012;41:1141-1149.
28. Soldatos T, Ahlawat S, Montgomery E, Chalian M, Jacobs MA, Fayad LM. Multiparametric assessment of treatment response in high-grade soft-tissue sarcomas with anatomic and functional MR imaging sequences. *Radiology*. 2016;278:831-840.
29. Usmanij EA, Natroshvili T, Timmer-Bonte JNH, et al. The predictive value of early in-treatment (18)F-FDG PET/CT response to chemotherapy in combination with bevacizumab in advanced nonsquamous non-small cell lung cancer. *J Nucl Med*. 2017;58:1243-1248.
30. Antoch G, Stattaus J, Nemat AT, et al. Non-small cell lung cancer: dual-modality PET/CT in preoperative staging. *Radiology*. 2003;229:526-533.
31. Benz MR, Evilevitch V, Allen-Auerbach MS, et al. Treatment monitoring by 18F-FDG PET/CT in patients with sarcomas: interobserver variability of quantitative parameters in treatment-induced changes in histopathologically responding and nonresponding tumors. *J Nucl Med*. 2008;49:1038-1046.
32. Fendler WP, Lehmann M, Todica A, et al. PET response criteria in solid tumors predicts progression-free survival and time to local or distant progression after chemotherapy with regional hyperthermia for soft-tissue sarcoma. *J Nucl Med*. 2015;56:530-537.

- 33.** Eary JF, O'Sullivan F, Powitan Y, et al. Sarcoma tumor FDG uptake measured by PET and patient outcome: a retrospective analysis. *Eur J Nucl Med Mol Imaging.* 2002;29:1149-1154.
- 34.** Schuetze SM, Rubin BP, Vernon C, et al. Use of positron emission tomography in localized extremity soft tissue sarcoma treated with neoadjuvant chemotherapy. *Cancer.* 2005;103:339-348.
- 35.** Herrmann K, Benz MR, Czernin J, et al. 18F-FDG-PET/CT Imaging as an early survival predictor in patients with primary high-grade soft tissue sarcomas undergoing neoadjuvant therapy. *Clin Cancer Res.* 2012;18:2024-2031.
- 36.** Byun BH, Kong CB, Lim I, et al. Combination of 18F-FDG PET/CT and diffusion-weighted MR imaging as a predictor of histologic response to neoadjuvant chemotherapy: preliminary results in osteosarcoma. *J Nucl Med.* 2013;54:1053-1059.

## Figures

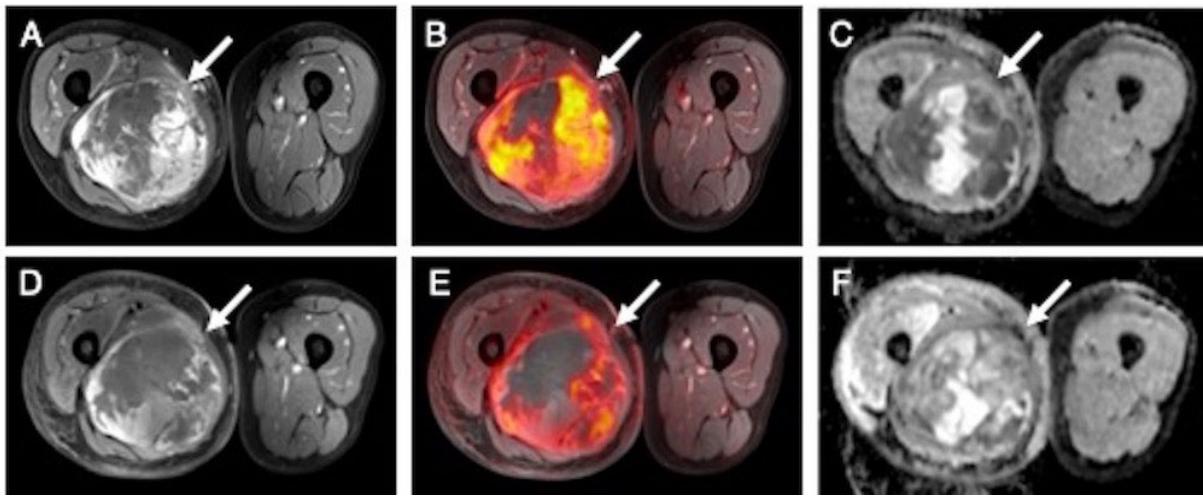


**FIGURE 1:** Pre- (a-c) and posttherapeutic (d-f) images of a 63 years-old patient with a STS (myxofibrosarcoma) of the right upper leg (arrows). The tumor size remains substantially stable after treatment (size: -1.1%; a and c, MRI), whereas the tumor reveals significant changes of the 18F-FDG uptake (SUVpeak: -60.4%; b and d, PET/MRI) and diffusion restriction (ADCmean: +37.4%; c and f, ADCmap). Histopathological analysis after surgical resection revealed a regression grade 3 (histopathological responder).

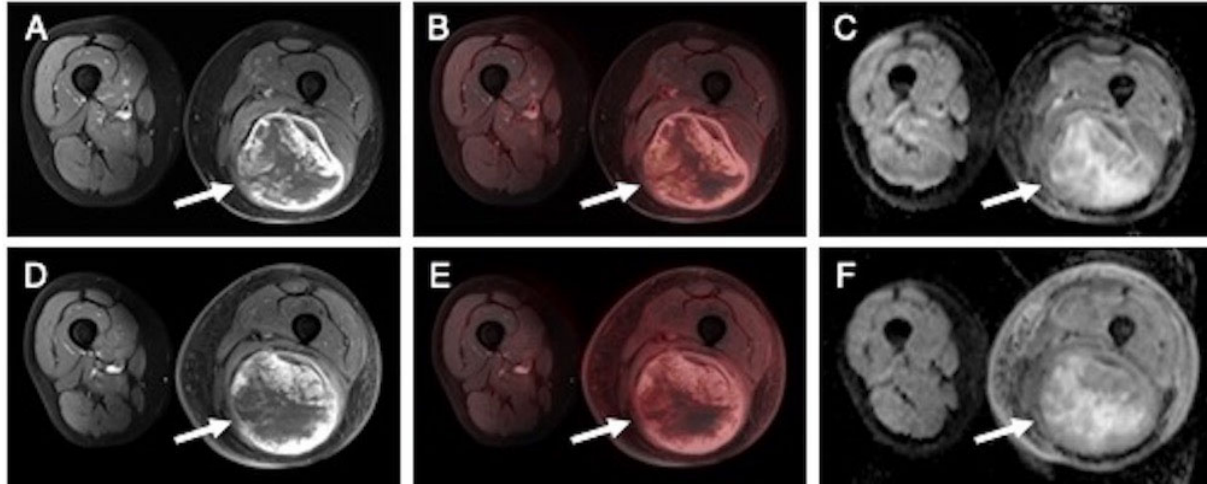


**FIGURE 2:** Images of a 56 years-old patient with a STS (leiomyosarcoma) of the left upper leg (arrows). The tumor does not show relevant changes in size (+5.3%; a and c, MRI), metabolic activity (SUVpeak: -7.7%, b and e, PET/MRI) and diffusion restriction (ADCmean: -5.1%, c and f, ADC-map) on pre- (a-c) and posttherapeutic (d-f) PET/MR images and was classified as histopathological non-responder (regression grade 5) after surgical resection.

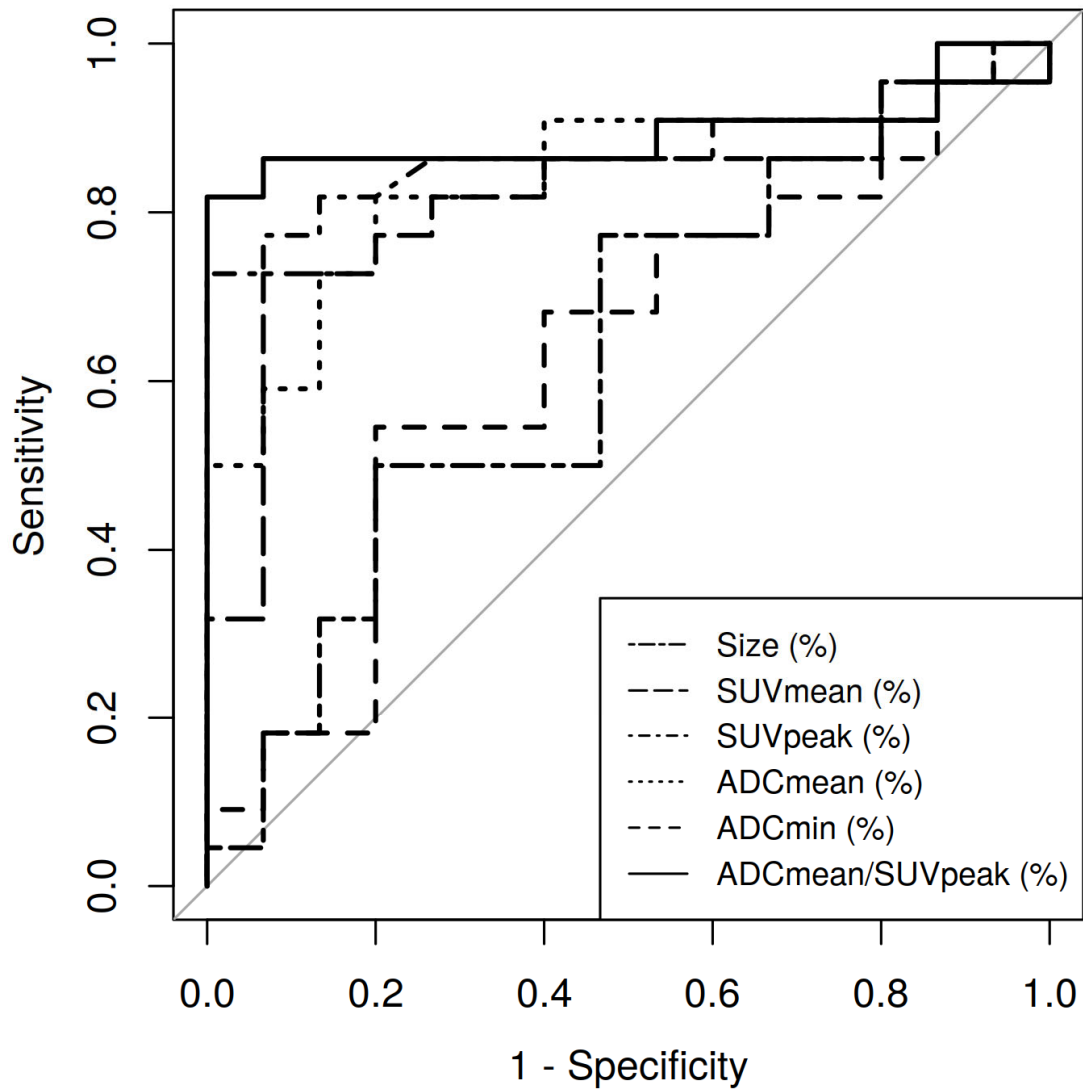


**FIGURE 3:** ROC-curves of the quantitative variables for the prediction of histopathological treatment response to ILP.

## Tables

<b>Histological subtype</b>	<b>Number of patients</b>
Undifferentiated pleomorphic sarcoma	9
Synovial sarcoma	9
Myxofibrosarcoma	6
Liposarcoma	6
Undifferentiated spindle cell sarcoma	3
Leiomyosarcoma	2
Epitheloid sarcoma	1
Malignant peripheral nerve sheath tumor	1
Total	37

**TABLE 1:** Histological subtypes of the soft tissue sarcomas.

<b>Regression grades</b>	<b>No. of patients</b>
Grade I	5
Grade II	5
Grade III	12
Grade IV	6
Grade V	8
Grade VI	1
Total	37

**TABLE 2:** Regression grades of all patients, according to the six-stage grading scale by Salzer-Kuntschik.

Parameter	Responder			Non-responder			P-values
	Mean values Pretherapeutic	Mean values Posttherapeutic	Percentage changes	Mean values Pretherapeutic	Mean values Posttherapeutic	Percentage changes	
Size	92.6±62.0	85.7±62.6	-9.7±9.8	114.6±59.5	108.7±61.8	-6.2±9.0	0.191
SUVmean	5.8±3.3	2.5±1.2	-43.8±35.6	2.9±1.3	2.5±1.5	-13.9±21.3	0.001
SUVpeak	8.6±4.6	3.4±1.8	-51.9±26.6	4.3±3.2	3.7±3.2	-17.3±17.9	< 0.001
ADCmin	568.3±156.0	708.7±173.6	+29.4±35.2	652.1±186.0	737.0±220.4	+15.3±29.1	0.202
ADCmean	1279.6±198.3	1678.7±196.6	+32.8±17.2	1412.1±277.9	1603.2±277.1	+14.6±10.2	< 0.001
ADCmean/ SUVpeak	225.8±189.4	628.1±298.2	+266.2±208.9	452.7±226.2	657.1±323.4	+43.2±26.6	< 0.001

**TABLE 3:** Results of quantitative image analysis for the different 18F-FDG PET and MR-derived imaging parameters

(mean values ± standard deviation).

Parameters	Size	SUVmean	SUVpeak	ADCmin	ADCmean	ADCmean/ SUVpeak
Size	<b>0.630</b>	0.150	0.036*	0.981	0.097	0.020*
SUVmean		<b>0.815</b>	0.295	0.117	0.803	0.151
SUVpeak			<b>0.871</b>	0.019*	0.690	0.150
ADCmin				<b>0.627</b>	0.024*	0.007*
ADCmean					<b>0.839</b>	0.463
ADCmean/ SUVpeak						<b>0.894</b>

**TABLE 4:** Results of ROC analysis. AUC values are shown in bold face. In addition, p-values indicating statistical differences (\*) between the different quantitative variables are given in the table.

	Plane	Slice thickness (mm)	Repetition time/ Echo time (ms)	Flip angle (°)	Field of view (mm)	Phase FoV (%)	Matrix size
<b>T1w VIBE Dixon</b>	coronal	3.12	3.6 / 1.23 (1 <sup>st</sup> ) and 2.46 (2 <sup>nd</sup> )	10	500	65.6	192 x 79
<b>STIR</b>	coronal	5	5990 / 57 Inversion time: 220ms	135	380	75.0	384 × 288
<b>T1w TSE</b>	axial	5	616 / 12	150	380	68.8	512 × 256
<b>T2w TSE</b>	axial	5	4860 / 106	150	380	68.8	512 × 256
<b>DW EPI (b-values: 0, 500, 1000 s/mm<sup>2</sup>)</b>	axial	5	7400 / 72	9	420	75.0	160 × 120
<b>T1w VIBE dynamic imaging fat saturated</b>	axial	3.5	4.32 / 2.21	9	380	68.8	512 × 308
<b>T1w TSE post contrast fat saturated</b>	coronal	5	542 / 13	160	380	75	512 × 256
<b>T1w TSE post contrast fat saturated</b>	axial	5	663 / 13	160	380	68.8	512 × 256

SUPPLEMENT TABLE 1: Illustration of the sequence parameters of the MR imaging protocol.

<b>Patient</b>	<b>Histological subtypes</b>	<b>Vital tumor (%)</b>	<b>Necrosis (%)</b>	<b>Fibrosis/Sclerosis (%)</b>	<b>Hemorrhage</b>
<b>1</b>	Undifferentiated pleomorphic sarcoma	5	60	35	+
<b>2</b>	Undifferentiated pleomorphic sarcoma	<1	70	<30	-
<b>3</b>	Undifferentiated pleomorphic sarcoma	<10	60	>30	+
<b>4</b>	Liposarcoma	90	10	0	-
<b>5</b>	Liposarcoma	20	30	50	-
<b>6</b>	Undifferentiated spindle cell sarcoma	<1	70	<30	-
<b>7</b>	Undifferentiated pleomorphic sarcoma	5	95	0	-
<b>8</b>	Undifferentiated pleomorphic sarcoma	40	50	10	+
<b>9</b>	Liposarcoma	80	20	0	-
<b>10</b>	Synovial sarcoma	5	90	5	-
<b>11</b>	Leiomyosarcoma	5	70	25	-
<b>12</b>	Myxofibrosarcoma	<10	70	>20	-
<b>13</b>	Synovial sarcoma	90	0	10	+
<b>14</b>	Undifferentiated spindle cell sarcoma	40	40	20	-
<b>15</b>	Undifferentiated spindle cell sarcoma	0	70	30	-
<b>16</b>	Synovial sarcoma	<1	30	<70	-
<b>17</b>	Undifferentiated pleomorphic sarcoma	<1	>90	<10	-
<b>18</b>	Synovial sarcoma	5	90	5	-
<b>19</b>	Myxofibrosarcoma	<10	60	>30	+
<b>20</b>	Synovial sarcoma	<1	60	<40	-
<b>21</b>	Synovial sarcoma	40	40	20	+

<b>22</b>	Myxofibrosarcoma	<10	80	>10	-
<b>23</b>	Liposarcoma	50	40	10	-
<b>24</b>	Myxofibrosarcoma	80	10	10	-
<b>25</b>	Undifferentiated pleomorphic sarcoma	0	70	30	-
<b>26</b>	Synovial sarcoma	40	30	30	-
<b>27</b>	Myxofibrosarcoma	100	0	0	-
<b>28</b>	Liposarcoma	<5	0	>95	-
<b>29</b>	Synovial sarcoma	0	60	40	+
<b>30</b>	Leiomyosarcoma	5	80	15	+
<b>31</b>	Epitheloid sarcoma	5	90	5	-
<b>32</b>	Undifferentiated pleomorphic sarcoma	0	0	100	-
<b>33</b>	Synovial sarcoma	50	40	10	-
<b>34</b>	Myxofibrosarcoma	90	0	10	-
<b>35</b>	Malignant peripheral nerve sheath tumor	<30	60	>10	-
<b>36</b>	Undifferentiated pleomorphic sarcoma	0	0	100	+
<b>37</b>	Liposarcoma	95	0	5	-

SUPPLEMENT TABLE 2: Illustration of the histological subtypes for all patients and histological results after tumor resection.